



Influence of water vapor distribution on the simulated track of Typhoon Hato (2017)

Jiaxin Chen^{1,2} · Chuying Mai¹ · Mingsen Zhou^{1,3} · Shumin Chen^{1,2} · Weibiao Li^{1,2} · Rong Fang¹ · Zhongkuo Zhao³

Received: 29 September 2020 / Accepted: 4 July 2021
© The Author(s) 2021

Abstract

Predicting tropical cyclone (TCs) tracks is a primary concern in TC forecasting. Some TCs appear to move in a direction favorable for their development, beyond the influence of the steering flow. Thus, we hypothesize that TCs move toward regions with high water-vapor content in the lower atmosphere. In this study, four numerical experiments, including a control experiment and three sensitivity experiments, were performed using the Weather Research and Forecasting Model, to analyze the relationship between water vapor distribution and the track of Severe Typhoon Hato (2017). Observations validated the features reproduced in the control experiment. The sensitivity experiments were conducted to explore variations in the TC track under different water vapor environments. Results indicate that the horizontal distribution of water-vapor content exerted a greater impact on the TC track than the steering flow when both factors were significant. Further analysis revealed that the TC's movement vector was between the direction of the steering flow and the direction toward the peak of vorticity increasing area. The peaks of vorticity increasing area were close to the peaks of water vapor increasing area, which also proved the effect of water vapor distribution on the TC track. These results are expected to improve TC track analysis and forecasting.

Keywords Tropical cyclone · Track · Water vapor distribution · Steering flow · Numerical simulation

1 Introduction

Predicting tropical cyclone (TC) tracks and landfall sites is a primary concern in TC forecasting in China, a country that often suffers serious TC-related disasters. TC tracks can be affected by various factors, and many previous studies have investigated the dynamic factors governing TC movements as they relate to TC track forecasting (Roy and Kovordányi 2012). These factors include the steering flow and the β -effect, with the former influencing TC tracks through the storms interactions with subtropical areas of high pressure, monsoon

✉ Shumin Chen
chenshm35@mail.sysu.edu.cn

Extended author information available on the last page of the article

systems, mid-latitude westerly troughs, and zonal winds in the mid-upper troposphere (George and Gray 1977; Chen and Chang 1980; Hodanish and Gray 1993; Chen et al. 2009; Wu and Chen 2016). However, some studies show that TCs appear to be influenced by both the dynamic and thermodynamic factors, since their movements can be studied through estimating potential vorticity (i.e., Wu et al. 2004). Therefore, other factors should be considered both in theoretical studies and in the practical forecasting of TC tracks.

Some TCs have reportedly shifted directions to travel in a way favorable for their development. Fisher (1958) indicated that TCs tend to follow tracks along the areas with the warmest water. Xu et al. (2013) identified that TCs, particularly some severe ones, exhibited the trend of making landfalls toward warmer land in China during 1960–2009 because a warmer surface provides moisture and energy to TCs. TCs typically intensify when they pass over warmer surface areas or encounter favorable environmental conditions in the lower atmosphere (Wang et al. 2001; Miglietta et al. 2011; Rai and Pattnaik 2018), particularly higher water-vapor content (WVC) (Krall and Cottrell 2012; Tsuboi et al. 2016; Khain et al. 2016). Herbener et al. (2014) reported that moist aerosols can initiate interactions between cloud microphysics and storm dynamics via latent heat release, thus leading to TC intensification. Many previous studies likewise reported that the latent heat released by water vapor is a major factor in TC development (Charney and Eliassen 1964; Fritz and Wang 2014; Hankes and Marinaro 2016; Chen et al. 2019). As heat released by the condensation of water vapor, mainly obtained from the surface layer, drives TC development (Emanuel 1991) and it has been observed that TCs can shift direction to favor development, it is possible that TCs may change track toward regions with high WVC.

Although water vapor is essential for TC development, few experimental or theoretical studies have investigated whether the horizontal distribution of water vapor affects TC tracks. In fact, studies about data assimilation and large-scale circulation have pointed out the effects of water vapor distribution on TC movements. Data assimilation is beneficial for obtaining the proper initial fields in numerical simulations (Roy and Kovordányi 2012). Many previous studies have shown that assimilating satellite-observed water vapor data can improve TC-track forecasting (i.e., Marshall et al. 1985; Marshall 1998; Deb et al. 2010; Yue et al. 2017; Chen and Zhang 2019). The interactions between water vapor distribution and TCs were usually related to large-scale system circulations, i.e., the water vapor distribution modified the TC's direction of movement because of its interaction with the monsoon gyre (Yan et al. 2017). Besides, TCs can lead to a decrease in water vapor content in the area that they move through (Francis et al. 2007).

The present study hypothesized that water-vapor content distribution can affect TC tracks, and examined the hypothesis through analyzing the Severe Typhoon Hato (2017) using the Weather Research and Forecasting (WRF) Model (Skamarock et al. 2008). Our previous study showed that the intensification of Hato was significantly affected by environmental water vapor (Wu et al. 2020). Hato developed over the western North Pacific, moved toward the west-northwest, and eventually made landfall on China's southern coast near Zhuhai (Guangdong Province), where it caused considerable loss of human life and substantial economic damage. At the time of landfall, the maximum wind speed near the TC center was 45 m s^{-1} and the minimum central pressure was 950 hPa, making it the most severe TC to affect China that year. To better understand the impact of regions with high water-vapor content on TC track, we conducted a control experiment and three sensitivity experiments. We anticipate that our results could be used to improve forecasting, thereby leading to more accurate TC track and intensity predictions in future.

2 Initial conditions and parameters for the numerical experiments

2.1 Control (CTL) experiment and validation

The CTL experiment was performed using the WRF Model, Version 3.8, which is among the best models currently available in terms of cyclone simulation performance (Panda et al. 2015; Islam et al. 2015; Hazelton et al. 2017; Chen et al. 2017). The initial fields and lateral boundary data used for the numerical simulation were derived from the initial fields of medium-range forecasts produced by the Regional Specialized Meteorological Center of the European Center for Medium-Range Weather Forecasts (hereafter ECMWF-RSMC data). The referenced dataset has a $0.125^\circ \times 0.125^\circ$ horizontal resolution, 18 vertical layers, and was recorded in 6-h time intervals. The Mercator projection was adopted for the double-nested domain used in the numerical experiment (Fig. 1). The coarse grid region (Domain 1) had 597×375 grids with grid intervals of 6 km. The fine grid region (Domain 2) had 1236×501 grids with intervals of 2 km. The boundary conditions, including the water vapor fluxes, were assigned the value from the ECMWF-RSMC data every six model hours for Domain 1, and obtained at every time step for Domain 2 from values in Domain 1 in the same region. There were 34 vertical layers and the top of the model was at a height of 50 hPa. The sea surface temperature (SST) was fixed during model integration. The WRF Single-Moment 6-Class microphysics scheme, Rapid Radiative Transfer Model longwave radiation scheme, Dudhia shortwave radiation scheme, Monin–Obukhov scheme, Noah land surface process scheme, and Yonsei University planetary boundary layer scheme were adopted in both domains. The Kain–Fritsch cumulus parameterization scheme was used only in Domain 1; no cumulus parameterization scheme was employed in Domain 2. The time of the simulation was set between 12:00 UTC August 21 and 12:00 UTC August 23, 2017.

The track of Hato simulated in CTL was compared with actual best-track data provided by the Shanghai Typhoon Institute of the China Meteorological Administration. The simulated TC motion (Fig. 2) was found to be generally consistent with the observed motion and the sites of TC landfall were similar. The observed TC intensity trends in the best-track data were also generally consistent with those simulated in the

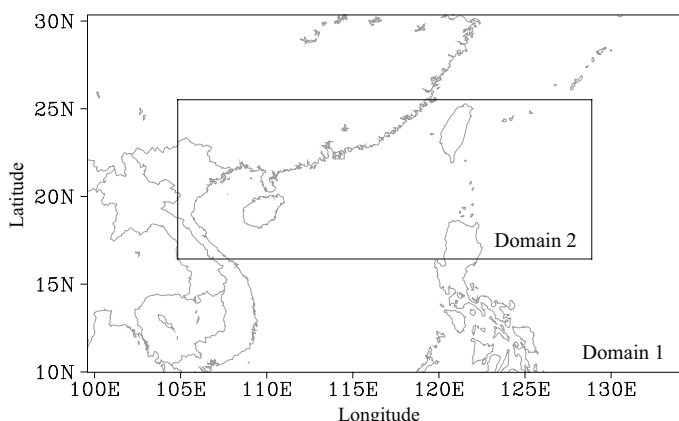


Fig. 1 Domain configuration used for the experiments

CTL, although the simulated TC intensity was slightly higher (Fig. 3). Possibly because the resolution of medium-range forecasts used for the integration for the initial field was relatively high (~13 km), and the initial field was not adjusted by assimilation or a bogus scheme, the initial TC was slightly deeper. The simulated minimum sea-level pressure in the CTL was generally consistent with that observed during the occurrence of the TC, except that the pressure in the CTL decreased faster and the simulated values were approximately 10 hPa lower than the observed values (Fig. 3a). The simulated maximum 10-m wind speed in the CTL was slightly higher than the observed values by an average of ~5–10 m s⁻¹ (Fig. 3b). The simulated precipitation was compared with NASA's Global Precipitation Measurement (GPM) Integrated Multi-satellite Retrievals for GPM (IMERG) precipitation data with a 0.1° × 0.1° horizontal resolution (Huffman et al. 2019) (Fig. 4). The comparison also showed that the CTL reasonably agreed with the observed data, except for the first 18 h (Fig. 4a–b) when the model was relatively unstable. Thus, the model performed satisfactorily in simulating Hato's track, intensity, and precipitation, and this numerical model was deemed suitable to investigate the effects of changes in water-vapor conditions on Hato's track. Figure 5a shows the evolution of both the radius of maximum wind (RMW) and the center tilt, defined as the horizontal distance between the TC center at sea level and the 6.6-km height of the simulated Hato. The RMW was 200 km at the beginning and decreased in an oscillatory manner to ~40 km as Hato intensified before model hour 21, after which RMW remained relatively stable. Meanwhile, the center tilt remained below 20 km after the TC entered the South China Sea at model hour 12 and became constant after model hour 21.

2.2 Sensitivity experiments

Three sensitivity experiments were conducted to explore the effects of different water vapor conditions on the TC track. The largest water vapor flux from the outer region to the model was derived from the southern lateral boundary of both Domain 1 and 2, for both the mean values of the troposphere and levels < 1.5 km (Fig. 6). Thus, the first and second sensitivity experiments modified the water vapor concentration at the southern lateral boundary of Domain 1 to double (hereafter, Double_SQ) and half (Half_SQ) in order to

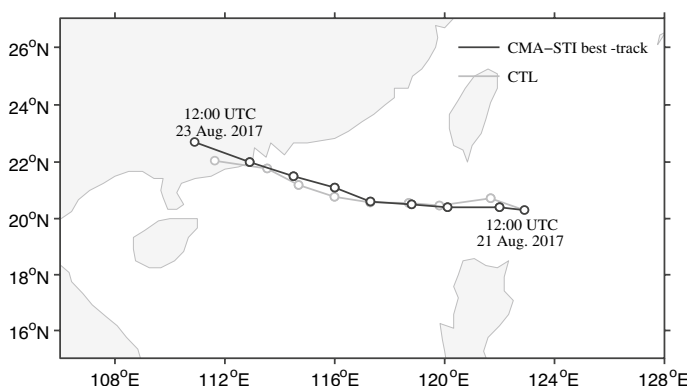
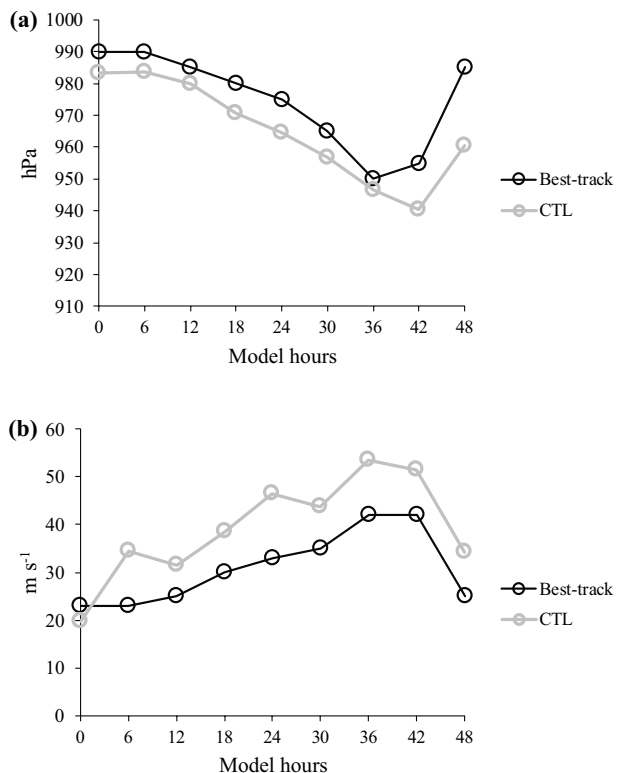


Fig. 2 Track of Typhoon Hato (2017) at 6-h intervals: Shanghai Typhoon Institute of the China Meteorological Administration (CMA-STI) best-track observations (black line) and the CTL experiment (gray line)

Fig. 3 Comparison of 6-h tropical cyclone intensity from the Shanghai Typhoon Institute of the China Meteorological Administration (CMA-STI) best-track dataset (black line) and control (CTL) simulation (gray line): **a** minimum sea level pressure (units: hPa) and **b** maximum 10-m wind speed (units: m s^{-1}) of Typhoon Hato (2017)



double and halve the existing water vapor flux at the boundary, respectively. Although the water vapor fluxes in the northern and eastern lateral boundary were also relatively large, it is worth noting that changing the water vapor fluxes at both the eastern and northern lateral boundary is not effective in modifying the water vapor distribution in the South China Sea, the main analyzed region, as the water vapor fluxes are affected by the nearby continents. Because of the impact of landmass, the amount of available water vapor mainly depends on the influx from the western North Pacific outside of the South China Sea, where the initial area of TC development lies. However, sensitivity experiments exploring changes in conditions of the eastern boundary can modify the initial TC structure by changing water vapor content available to the TC during its initial stages, which can add uncertainty to the analysis. As a result, only the water vapor content in the south lateral boundary of Domain 1 was modified in the first two experiments to construct a more stable Domain 2, the domain of primary focus in analysis. Changes to this boundary propagate across the space between the southern lateral border of each domain, resulting in a different but more stable set of conditions for the southern boundary of Domain 2. For the third sensitivity experiment (hereafter, Con_Q), the initial WVC was changed uniformly to the horizontal mean value of the simulated regional space at the same height. Except for the settings mentioned above, all other settings for the sensitivity experiments, including the boundary conditions, were the same as those used in the CTL.

Figure 5b-d shows the evolution of the RMW and center-tilt in the three sensitivity experiments. The RMW and tilt were similarly stable after model hour 21 in the sensitivity

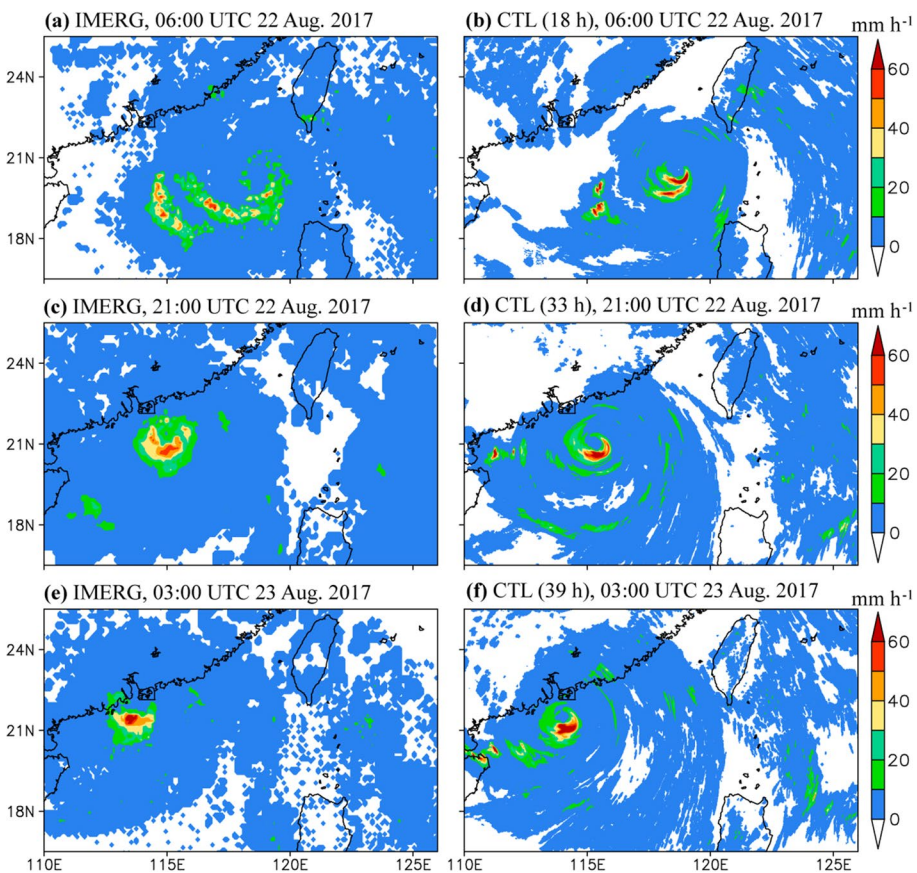


Fig. 4 Comparison of observed and simulated precipitation rate (units: mm h^{-1}) of Typhoon Hato (2017): **a, c, e** NASA Global Precipitation Measurement (GPM) Integrated Multi-satellite Retrievals for GPM (IMERG) precipitation data and **b, d, f** control (CTL) experiment

experiments, although their variations were not as stable as those in the CTL. Thus, based on the comparison of precipitation data to those of the CTL, most of the following analysis focuses on simulation results after model hour 21, when the TC was reasonably stable and its track was less affected by factors related to its inner structure. The present study focused on the relationship between the horizontal distribution of WVC within the lower atmosphere and the simulated track of Hato. The evolution of the horizontal distribution of WVC and large-scale circulation related to the steering flow in each experiment were not analyzed in the present study, but they should be studied in detail in future.

3 Results

3.1 Evolution of the horizontal distribution of WVC

The distribution of mean WVC, averaged in the time range of 0–48 h, in the lower atmosphere in the four experiments was analyzed (Fig. 7). The horizontal distribution of WVC

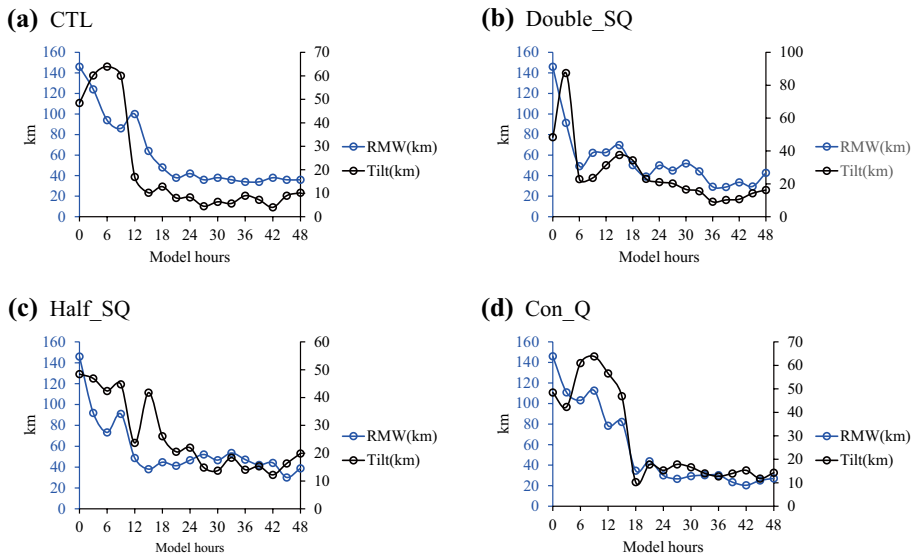


Fig. 5 The 3-hourly radius of maximum wind (RMW; blue line; units: km) and center tilt between sea level and 6.6 km height (black line; unit: km) of the simulated Typhoon Hato (2017) in the control (CTL) experiment

Fig. 6 Mean water vapor flux (unit: $\text{kg m kg}^{-1} \text{s}^{-1}$) at the four lateral boundaries of the control (CTL) experiment. Positive values represent inward flux from outer regions. Blue bars represent the mean values of all levels in troposphere and orange bars represent the mean values at the height $< 1.5 \text{ km}$. **a** for Domain 1, and **b** for Domain 2, respectively

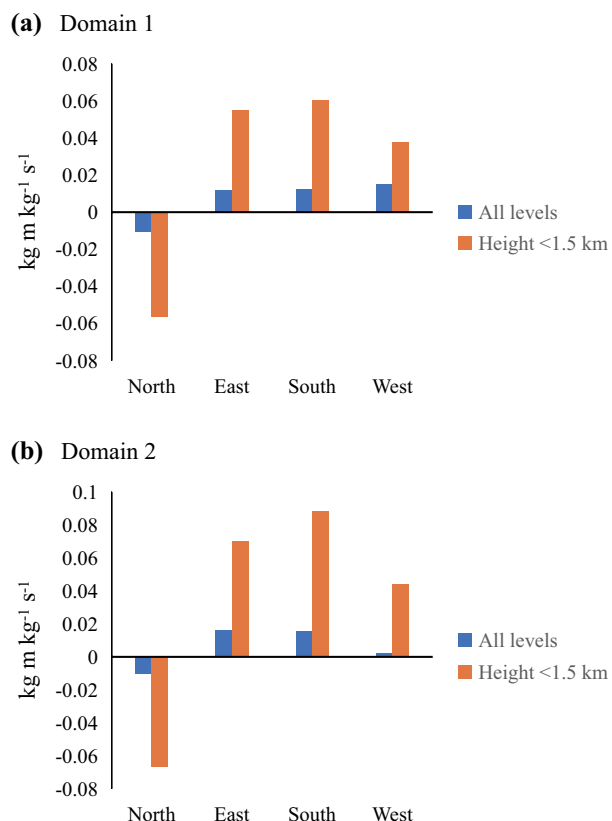


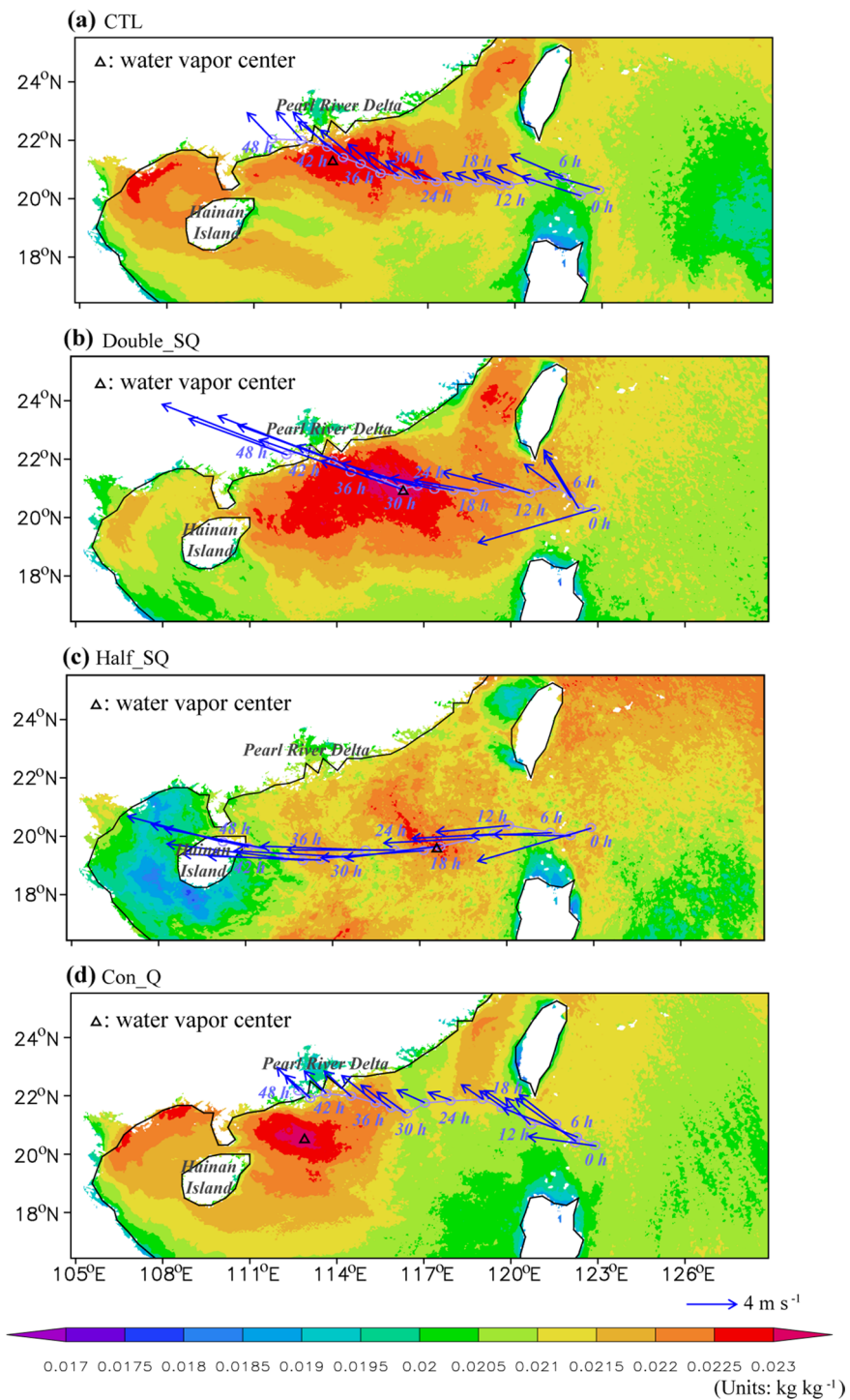
Fig. 7 Distribution of water-vapor content (shading; units: kg kg^{-1}), averaged in 0–48 h, in the lower atmosphere ($z=49.97 \text{ m}$) and steering flow (vectors; units: m s^{-1}) at the tropical cyclone center: **a** control (CTL) and sensitivity experiments: **b** Double_SQ, **c** Half_SQ, and **d** Con_Q. Purple lines with open circles indicate the simulated tropical cyclone track at 3-h intervals, and their times were marked 6 hourly by the purple characters. The black triangles mark the centers of water-vapor content

was similar in CTL, Double_SQ, and Con_Q and was characterized by a center of high water-vapor content (HWVC center) located near the coastline of the Pearl River Delta. Compared with its position in CTL, this HWVC center was approximately 2.26° further east in Double_SQ and approximately 0.82° further east and 0.72° further south in Con_Q. The HWVC center was larger in Double_SQ than in the other experiments because the water vapor transported into the model at the southern lateral boundary was doubled, whereas in Half_SQ it was the weakest because the water vapor transported into the model at the southern lateral boundary was halved. The HWVC located near the coastline of the Pearl River Delta disappeared in Half_SQ, although a weak center remained at approximately 20° N , 117° E .

The evolution of instantaneous WVC was further analyzed (Fig. 8). Owing to the difficulty to capture the environmental distribution of WVC and analyze the unaveraged components, which is dominated by TC signals, the WVC was low-passed filtered after standardization, based on the Kurihara filter method (Kurihara et al. 1990, 1993). Although the HWVC centers related to the location of the TC were not fully filtered out, there still existed HWVC centers located near the coastline of the Pearl River Delta in experiments other than Half_SQ (please refer to the first and second columns in Fig. 8). The locations of these HWVC centers being close to their mean location in Fig. 7 suggests that the fields of WVC shown are representative, although these HWVC centers weakened after TCs passed through them (third column in Fig. 8).

3.2 Horizontal distribution of WVC, steering flow, and TC track

As shown in Fig. 7, the steering flow, estimated based on the approach of Peng et al. (2015), was similar in CTL and Con_Q because the lateral boundary conditions were similar. However, unlike the horizontal WVC in the lower layer, the steering flow in Double_SQ was not similar to that in CTL and Con_Q. The steering flow was approximately twice that of the CTL and Con_Q experiments and was more westward, which could be because of the large-scale circulation controlling the steering flow which was modified by the changed lateral boundary conditions of Double_SQ. The magnitude of the steering flow in Half_SQ, which was also affected by the modified lateral boundary conditions, was similar to that in Double_SQ, though the direction of the steering flow was more southwestward than in Double_SQ compared to CTL. The large-scale circulations in these two experiments were generally modified by the change of geopotential field near the TC (Fig. 9). The atmospheric mass and heat content, affected by the differences in water vapor content, increased and decreased in the southern part of the models, respectively, contributing to the enhanced north-southward pressure gradient (Fig. 10). Here, only the initial (9 h) and final (48 h) stages of the simulation were analyzed in Fig. 10, to avoid the noise from the TC. The contours of geopotential height in Double_SQ/Half_SQ turned more west-eastward from north-southward in CTL, which enhanced the north-south pressure gradient, and then enhanced the meridional component of the winds. Thus, the steering flow in these two experiments changed compared to the CTL. Additionally, Fig. 9 shows that TCs



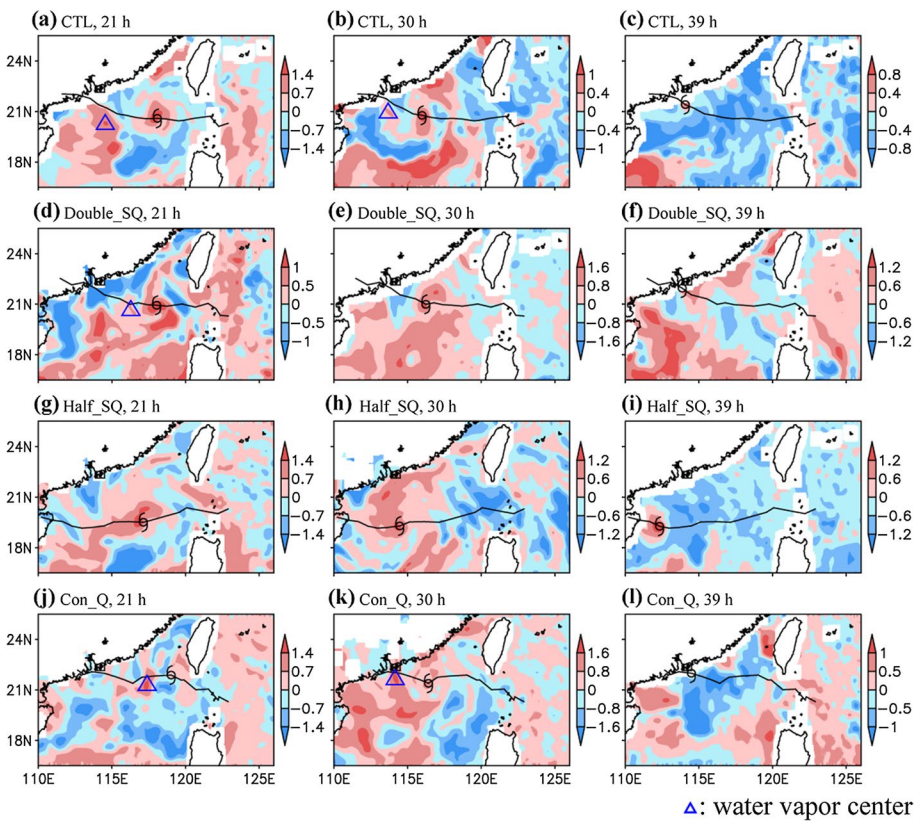


Fig. 8 Evolution of low-passed filtered standardized water-vapor content (shading), with **a–c** for CTL, **d–f** for Double_SQ, **g–h** for Half_SQ and **j–l** for Con_Q experiment, respectively; and with **a, d, g and j** for 21 h, **b, e, h and k** for 20 h, and **c, f, i and l** for 39 h, respectively. Black lines indicate the simulated tropical cyclone track, with marks indicating the location of tropical cyclone at the moment. The blue triangles (“ Δ ”) mark the centers of water-vapor content

in Double_SQ/Half_SQ were generally moving along the isobar, although the movement direction of TC in Double_SQ was divided from the direction of steering flow, which was estimated from a larger area.

It is worth noting that Fig. 9 shows the mean pressure gradient in Half_SQ which was much higher than that in Double_SQ, but this feature was not visible in the instantaneous fields (Fig. 10). Considering that features in Fig. 9 were also affected by the evolution of TC, we believe that the interaction between the modified water vapor field and TC evolution is worth discussing and deserves a more detailed analysis in future. Furthermore, the response of the geopotential height is opposite between Double_SQ and Half_SQ. For Double_SQ, the enhanced geopotential height was pushed northward by the TC, and then a closed area of high pressure was established (the isobar of 5900 hPa) near 21° N, and thus the north-south pressure gradient was enhanced at the southern part of the model (Fig. 10a). For Half_SQ, the decrease of geopotential height at the southern part of the model directly turned the contours of geopotential height more west-eastward compared to CTL (Fig. 10c).

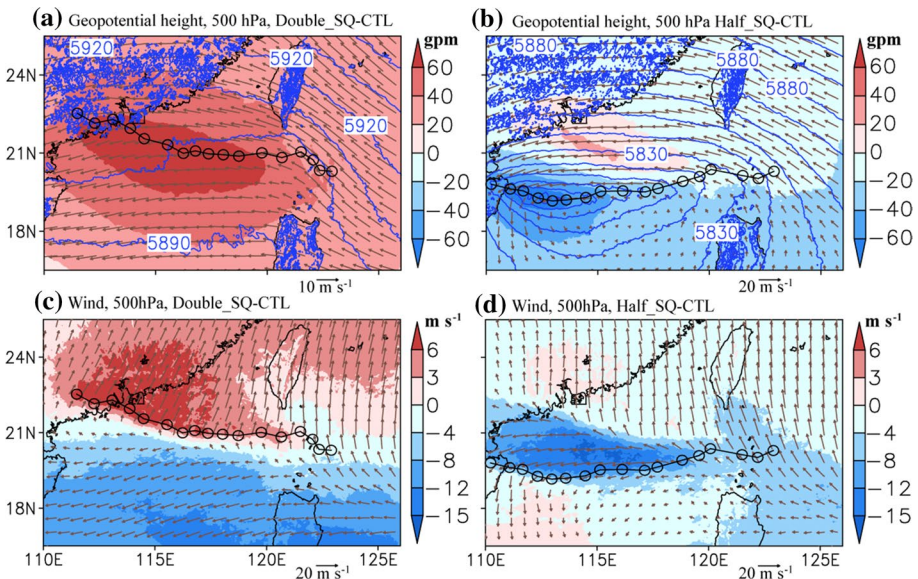


Fig. 9 Differences of large-scale fields of pressure and winds between Double_SQ/Half_SQ and CTL, averaged in 0–48 h. **a** and **b** show the difference of geopotential height (shading; unit: gpm) in 500 hPa level between Double_SQ and CTL, and Half_SQ and CTL, respectively. Blue contours and brown vectors respectively show the geopotential height (unit: gpm) and wind vectors (unit: m s^{-1}) in **a** Double_SQ and **b** Half_SQ. **c** and **d** show the difference of zonal wind (shading; unit: m s^{-1}) and wind vectors (brown vector; unit: m s^{-1}) in 500 hPa level between Double_SQ and CTL, and Half_SQ and CTL, respectively. Black lines with open circles indicate the simulated tropical cyclone track at 3-h intervals

As with the similar horizontal distribution of the lower-layer WVC, the TC track was similar in CTL, Double_SQ, and Con_Q, in that the TC landfall was in the Pearl River Delta region of southern China in each of these experiments. Before passing nearest to the HWVC center, the TC track in both CTL and Double_SQ deviated from the direction of the steering flow. Thus, the TC tracks in these two experiments were between the direction of the steering flow and the direction from the TC center to the HWVC center. After deviation from the HWVC center (TC passed through the HWCV at ~36 h for CTL and ~30 h for Double_SQ), the TC track in each experiment was more consistent with that of the direction of the steering flow. As the HWVC center in the Con_Q experiment was located further west, it was always in front of the TC before the TC made landfall. Thus, the TC track in this experiment always deviated considerably from the direction of the steering flow. Relative to the TC tracks in the other experiments, the TC track in the Half_SQ experiment was more southerly, and the TC made landfall over Hainan. During 12–21 h, the TC in Half_SQ moved southwestward toward the HWVC center, after which its direction of movement was more consistent with the direction of the steering flow. Thus, in each of the experiments, the simulated track of Hato was affected by both the steering flow and the horizontal distribution of the lower-layer WVC, and the track tended to be closer to the direction toward the HWVC center.

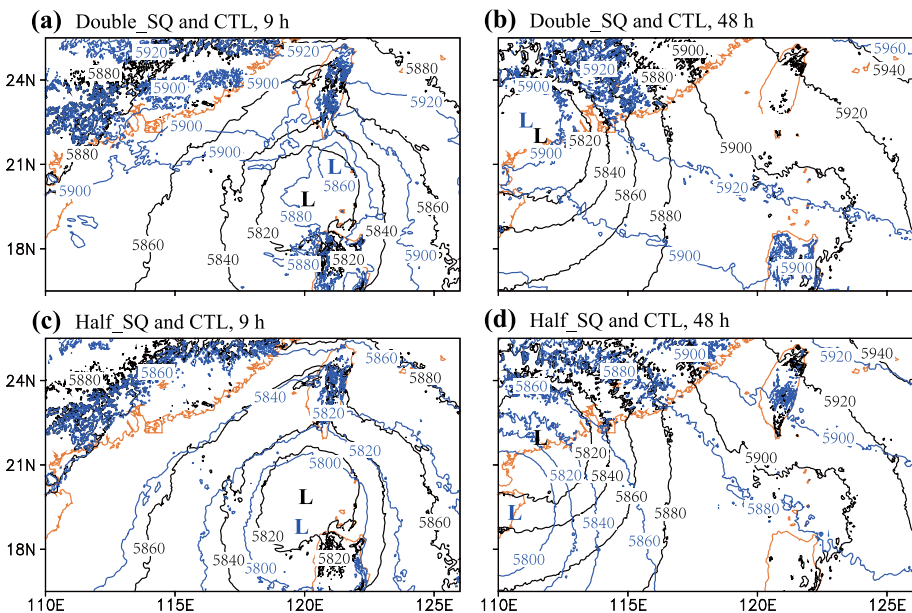


Fig. 10 Geopotential height (contours; unit: gpm) in 500 hPa level for **a**, **b** Double_SQ (blue) and CTL (black), and **c**, **d** Half_SQ (blue) and CTL (black). **a**, **c** and **b**, **d** show the 9 and 48 h, respectively. Here, the symbol “L” indicates the main area of TC

3.3 Directions from TC track to steering flow and HWVC

The angles between the direction of the temporal HWVC center and the direction of TC motion (α) and that between the direction of the steering flow and TC motion (β) were estimated (Fig. 11). During the period after model hour 21 and 6 h before landing, the TC track was between the direction of the steering flow and that toward the HWVC center in CTL, Double_SQ, and Con_Q. The TC tracks in each of these experiments were closer to the direction of the HWVC center, that is, the values of α were approximately $2^\circ\text{--}7^\circ$ smaller than those of β . For the TC simulated in CTL and Double_SQ, the value of β decreased from 20° to 30° to 10° after the TC passed through the HWVC center, at ~ 36 h for CTL and ~ 30 h for Double_SQ. This suggests that the TC track was close to the direction of the steering flow when the HWVC center was not in front of the TC. In Half_SQ, the TC deviated from the HWVC center at the model hour 18; thus, the value of α was missing after this time. Thus, its track was close to the direction of the steering flow, with a β value of $\sim 10^\circ$ for nearly the entire period after model hour 21 and 6-h before landing. In summary, although the simulated track of Hato was controlled by the steering flow, it tended to be more affected by the horizontal distribution of WVC than by the steering flow when both factors were significant. Note that the TC evolution was relatively unstable before model hour 21 (also analyzed in Fig. 5) and after 6-h before landing; the values of the angles were relatively larger and the angle variations of that were relatively unstable.

The relation between the distribution of WVC and TC structure, and the related TC motion, remain to be debated. For example, in the studies of Fujiwara et al. (2020), a TC can weaken independent of the evaporation nearby being increased or decreased. Thus,

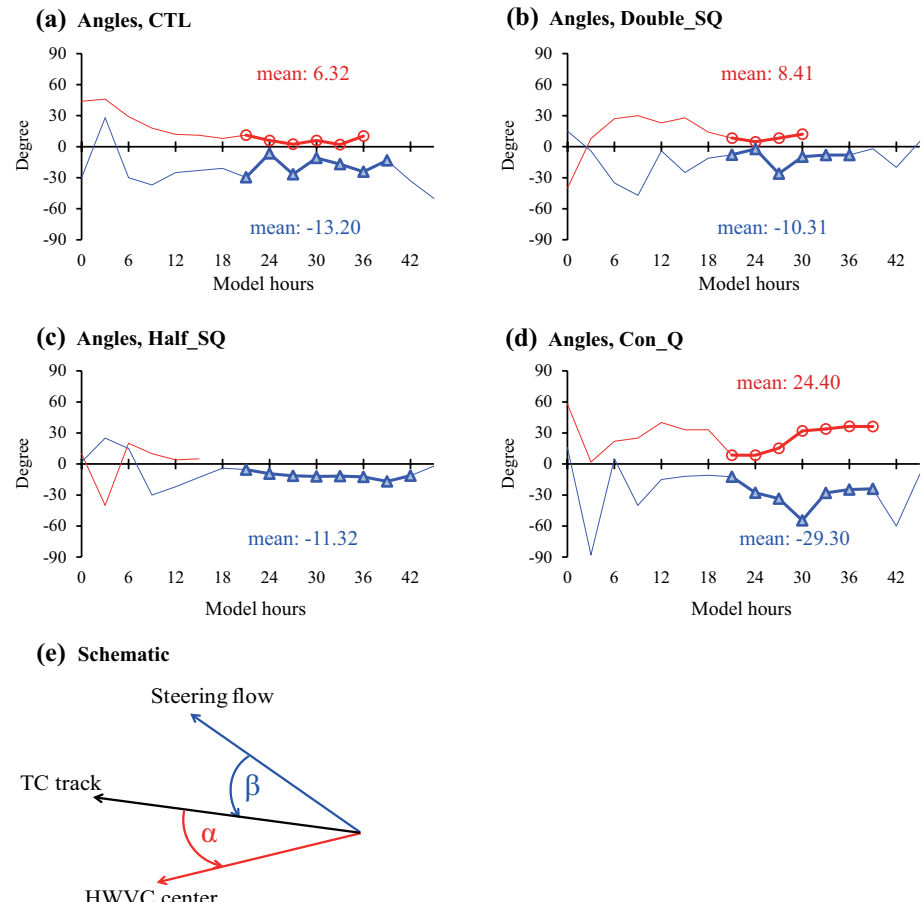


Fig. 11 Angle between the direction toward the center of high water-vapor content (HWVC center) (i.e., the line connecting the maximum temporal water-vapor content and the tropical cyclone (TC) center) and the direction of TC motion (α ; red; units: degrees), and the angle between the directions of the steering flow and TC motion (β) (blue; units: degrees), averaged during the period from 21 to 6 h before landfall: **a** control (CTL) and sensitivity experiments **b** Double_SQ, **c** Half_SQ, and **d** Con_Q. Positive values represent counterclockwise angles. **e** Schematic showing method of estimation of the two angles (α and β). Based on Fig. 6 and in order to avoid the effect of the proximity of land on the TC track, the period after model hour 21 and 6-h before landing was highlighted by thick lines with marks in the first four figures. For **a**, **b**, and **c**, the values of α were missing for the final few intervals of the period primarily because the TC had passed the point of its nearest approach to the HWVC center

analysis on the tendency of absolute vertical vorticity was performed based on Yamada et al. (2016) (Fig. 12), which shows that the positive peak of absolute vertical vorticity tendency exists in the same direction as the TC motion. The absolute vertical vorticity can be expressed as $(\zeta + f)$, where ζ and f , respectively, are the vertical advection of the relative vorticity and advection of the Coriolis parameter. Results show that the TC direction of movement was between the direction of the steering flow and that toward the peak of vorticity increasing area. Positive peaks of vorticity tendency ($\frac{\partial(\zeta+f)}{\partial t}$) were mainly located in the southwest quarter of the TC and close to the TC center at both low and high layers,

Fig. 12 The absolute vertical vorticity tendency ($\frac{\partial(\zeta+f)}{\partial t}$) (shading; unit: 10^{-9} s^{-2}) and water vapor tendency ► (brown contour; dashed line for zero value, solid line with interval and minimum value of both 0.8; unit: $10^{-9} \text{ kg kg}^{-1} \text{ s}^{-1}$) within the radius of 200 km around the TC center at model hour 21. **a, c, e and g** for 850 hPa, and **b, d, f and h** for 300 hPa, respectively. **a** and **b** for CTL, **c** and **d** for Double_SQ, **e** and **f** for Half_SQ, and **g** and **h** for Con_Q, respectively. Black vector indicates the direction of TC motion, and blue dashed vector indicates the direction of steering flow

except for the 300 hPa level in Double_SQ. The peaks of vorticity increasing area were close to the peaks of water vapor increasing area, with the contours concentrated near the positive peaks of $\frac{\partial(\zeta+f)}{\partial t}$, and mainly in the southwest quarter of the TC. This further demonstrates the effect of water vapor distribution on the TC track. Note that the fields of $\frac{\partial(\zeta+f)}{\partial t}$ was noisier, further analysis about the vorticity fields is required to obtain more detailed physical links between vorticity and TC motions.

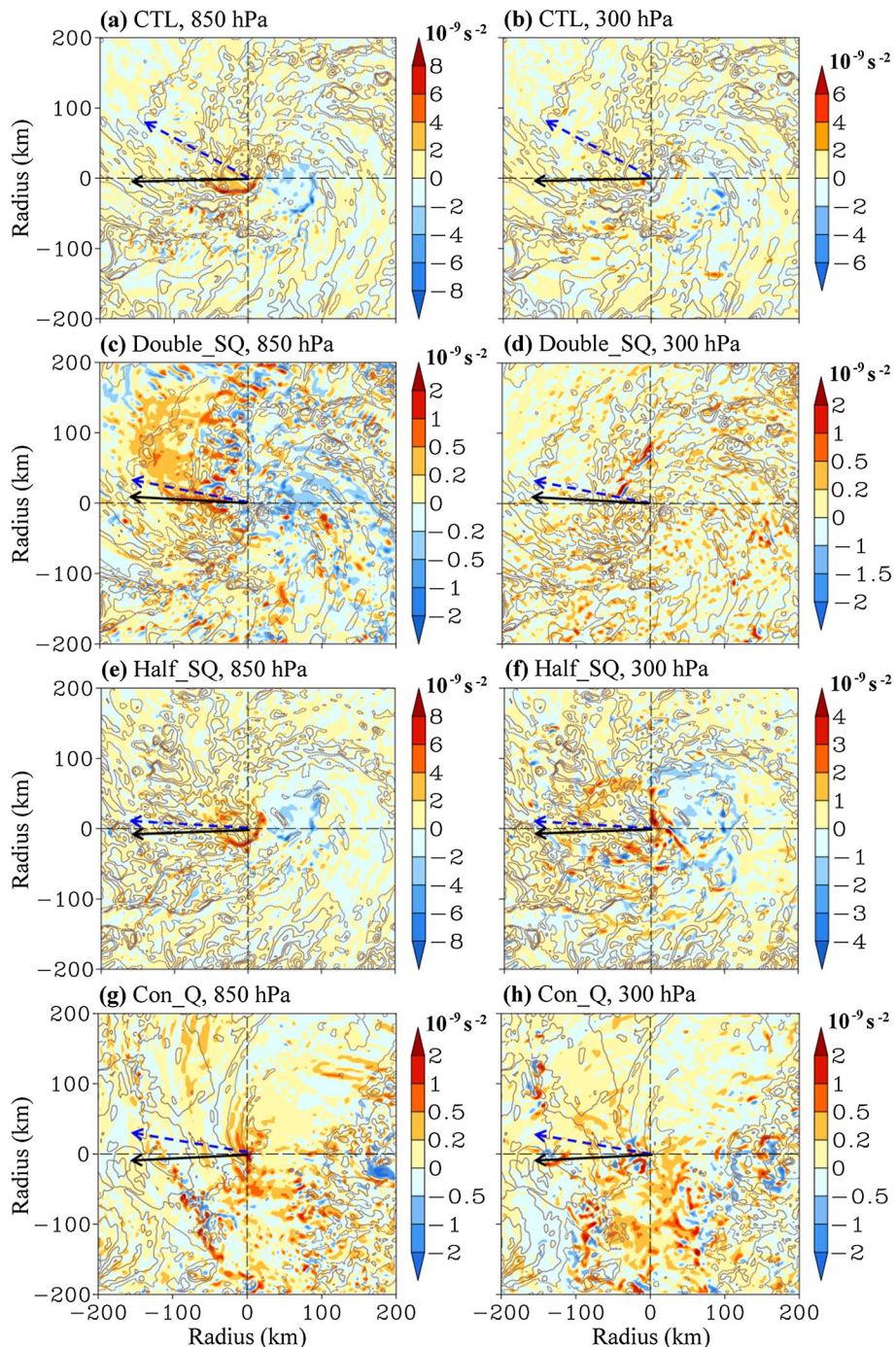
4 Conclusions

Predicting TC tracks is a primary concern in TC forecasting in China, which often suffers from the serious consequences of TC disasters at TC landfall locations. Beyond the influence of the steering flow, a TC often tracks in a direction favorable for their development, particularly toward HWVC centers in the lower atmosphere. This study used the WRF Model to perform a control experiment (CTL; based on actual data from Typhoon Hato) and three sensitivity experiments (Double_SQ, Half_SQ, and Con_Q) to analyze the relationship between the horizontal distribution of water vapor in the lower layer and the track of Hato. The water vapor flux at the southern lateral boundary of the model was doubled and halved in Double_SQ and Half_SQ, respectively. The initial water vapor in the Con_Q experiment was set uniformly to the horizontal averaged value of the simulated regional space at each height.

Analyses of the relationships among the horizontal atmospheric WVC distribution, steering flow, and TC track in the four experiments revealed that the simulated track of Hato was more influenced by the horizontal distribution of WVC than by the steering flow when both these factors were significant. The TC track was close to the direction of the steering flow only when no HWVC center was present in front of the TC. Detailed analyses show that the TC moving direction was between the direction of the steering flow and that toward the peak of vorticity increasing area, while the peaks of vorticity increasing area were close to the peaks of water vapor increasing area. This suggests that WVC in the low layer was one of the factors influencing TC tracks, although it is insufficiently discussed in previous studies. These findings may help improve the predictions of TC track and intensity in the future, thereby aiding in preventing property damage and loss of life.

The present study was intended as a preliminary analysis of the potential relationship between the distribution of water vapor and the track of Typhoon Hato. Thus, some of the detailed physical mechanisms are not fully considered, i.e., the relationship between water vapor transport and the formation of convection in TCs and how this relationship might affect the TC motion. Both dynamic and thermodynamic analyses are required in future studies to clarify these mechanisms.

Acknowledgements We thank James Buxton MSc from Liwen Bianji, Edanz Group China (<https://en-author-services.edanzgroup.com>) for English-language editing.



Authors' contributions Conceptualization: Shumin Chen, Weibiao Li; Methodology: Jiaxin Chen, Chuying Mai; Formal analysis and investigation: Mingsen Zhou, Rong Fang, Jiaxin Chen; Writing - original draft preparation: Jiaxin Chen, Chuying Mai; Writing - review and editing: Shumin Chen; Funding acquisition: Shumin Chen, Weibiao Li, Zhongkuo Zhao; Supervision: Shumin Chen.

Funding This work was supported by the Fundamental Research Funds of the Guangzhou Science and Technology Plan Project [Grant No. 201903010036], China Postdoctoral Science Foundation [Grant No. 2020M683021], National Natural Science Foundation of China [Grant Nos. 42075004, 41875021, and 41830533], and National Innovation training program for students of Sun Yat-sen University [Grant No. 201801191].

Data availability The actual TC best-track data provided by the Shanghai Typhoon Institute of the China Meteorological Administration are available at <http://www.typhoon.org.cn>. The Tropical Rainfall Measuring Mission 3B42 RT precipitation data are available at <https://pmmm.nasa.gov/data-access/downloads/trmm>. The initial and boundary conditions of the numerical experiments are from the medium-range forecasts produced by the Regional Specialized Meteorological Center of the European Center for Medium-Range Weather Forecasts (<https://www.ecmwf.int>). The simulation results from the WRF Model are available upon request; please contact Shumin CHEN (es04csm@mail2.sysu.edu.cn) for details.

Declarations

Conflicts of interest The authors declare that they have no conflicts of interest.

Open Access This article is licensed under a Creative Commons Attribution 4.0 International License, which permits use, sharing, adaptation, distribution and reproduction in any medium or format, as long as you give appropriate credit to the original author(s) and the source, provide a link to the Creative Commons licence, and indicate if changes were made. The images or other third party material in this article are included in the article's Creative Commons licence, unless indicated otherwise in a credit line to the material. If material is not included in the article's Creative Commons licence and your intended use is not permitted by statutory regulation or exceeds the permitted use, you will need to obtain permission directly from the copyright holder. To view a copy of this licence, visit <http://creativecommons.org/licenses/by/4.0/>.

References

- Charney JG, Eliassen A (1964) On the growth of the hurricane depression. *J Atmos Sci* 21(1):68–75. [https://doi.org/10.1175/1520-0469\(1964\)021<0068:OTGOTH>2.0.CO;2](https://doi.org/10.1175/1520-0469(1964)021<0068:OTGOTH>2.0.CO;2)
- Chen S, Li W, Wen Z, Lu Y, Zhou M, Qian YK, Chen G (2019) Vertical motions prior to the intensification of simulated Typhoon Hagupit (2008). *J Geophys Res: Oceans* 124(1):577–592. <https://doi.org/10.1029/2018JC014086>
- Chen TC, Wang SY, Yen MC, Clark AJ (2009) Impact of the intraseasonal variability of the western North Pacific large-scale circulation on tropical cyclone tracks. *Weather Forecast* 24(3):646–666. <https://doi.org/10.1175/2008WAF2222186.1>
- Chen TJ, Chang CP (1980) The structure and vorticity budget of an early summer monsoon trough (Mei-Yu) over southeastern China and Japan. *Mon Weather Rev* 108(7):942–53. [https://doi.org/10.1175/1520-493\(1980\)108<0942:TSAVBO>2.0.CO;2](https://doi.org/10.1175/1520-493(1980)108<0942:TSAVBO>2.0.CO;2)
- Chen X, Wang Y, Zhao K, Wu D (2017) A numerical study on rapid intensification of Typhoon Vicente (2012) in the South China Sea. Part I: verification of simulation, storm-scale evolution, and environmental contribution. *Mon Weather Rev* 145(3):877–898. <https://doi.org/10.1175/MWR-D-16-0147.1>
- Chen X, Zhang F (2019) Development of a convection-permitting air-sea-coupled ensemble data assimilation system for tropical cyclone prediction. *J Adv Model Earth Sy* 11:3474–3496. <https://doi.org/10.1029/2019MS001795>
- Deb SK, Kishtawal CM, Pal PK (2010) Impact of Kalpana-1-derived water vapor winds on Indian Ocean tropical cyclone forecasts. *Mon Weather Rev* 138(3):987–1003. <https://doi.org/10.1175/2009MWR3041.1>
- Emanuel K (1991) The Theory Of Hurricanes. *Annu Rev Fluid Mech* 23:179–196. <https://doi.org/10.1146/annurev.fl.23.010191.001143>

- Francis PA, Gadgil S, Vinayachandran PN (2007) Triggering of the positive Indian Ocean dipole events by severe cyclones over the Bay of Bengal. *Tellus A* 59:461–475. <https://doi.org/10.1111/j.1600-0870.2007.00254.x>
- Fisher EL (1958) Hurricanes and the Sea-Surface Temperature Field. *J Atmos Sci* 15: 328–333. [https://doi.org/10.1175/1520-0469\(1958\)015<0328:HATSST>2.0.CO;2](https://doi.org/10.1175/1520-0469(1958)015<0328:HATSST>2.0.CO;2)
- Fujiwara F, Kawamura R, Kawano T (2020) Suppression of tropical cyclone development in response to a remote increase in the latent heat flux over the Kuroshio: a case study for Typhoon Chaba in 2010. *SOLA* 16:151–156
- Fritz C, Wang Z (2014) Water vapor budget in a developing tropical cyclone and its implication for tropical cyclone formation. *J Atmos Sci* 71(11):4321–4332. <https://doi.org/10.1175/JAS-D-13-0378.1>
- George JE, Gray WM (1977) Tropical cyclone recurvature and nonrecurvature as related to surrounding wind-height fields. *J App Meteorol* 16(1):34–42. [https://doi.org/10.1175/1520-0450\(1977\)016<0034:TCRANA>2.0.CO;2](https://doi.org/10.1175/1520-0450(1977)016<0034:TCRANA>2.0.CO;2)
- Hankes I, Marinaro A (2016) The impacts of column water vapour variability on Atlantic basin tropical cyclone activity. *Q J R Meteorol Soc* 142(701):3026–3035. <https://doi.org/10.1002/qj.2886>
- Hazelton AT, Hart RE, Rogers RF (2017) Analyzing simulated convective bursts in two Atlantic hurricanes. Part II: intensity change due to bursts. *Mon Weather Rev* 145(8):3095–3117. <https://doi.org/10.1175/MWR-D-16-0268.1>
- Herbener SR, Van Den Heever SC, Carrión GG, Saleeby SM, Cotton WR (2014) Aerosol indirect effects on idealized tropical cyclone dynamics. *J Atmos Sci* 71(6):2040–2055. <https://doi.org/10.1175/JAS-D-13-0202.1>
- Hodanish S, Gray WM (1993) An observational analysis of tropical cyclone recurvature. *Mon Weather Rev* 121(10):2665–89. [https://doi.org/10.1175/1520-0493\(1993\)121<2665:AOAOTC>2.0.CO;2](https://doi.org/10.1175/1520-0493(1993)121<2665:AOAOTC>2.0.CO;2)
- Huffman GJ, Stocker EF, Bolvin DT, Nelkin EJ, Tan J (2019) GPM IMERG Final Precipitation L3 Half Hourly 0.1 degree x 0.1 degree V06, Greenbelt, MD, Goddard Earth Sciences Data and Information Services Center (GES DISC). <https://doi.org/10.5067/GPM/IMERG/3B-HH/06>
- Islam T, Srivastava PK, Rico-Ramirez MA, Dai Q, Gupta M, Singh SK (2015) Tracking a tropical cyclone through WRF–ARW simulation and sensitivity of model physics. *Nat Hazard* 76(3):1473–1495. <https://doi.org/10.1007/s11069-014-1494-8>
- Khai A, Lynn B, Shpund J (2016) High resolution WRF simulations of Hurricane Irene: sensitivity to aerosols and choice of microphysical schemes. *Atmos Res* 167:129–145. <https://doi.org/10.1016/j.atmosres.2015.07.014>
- Krall GM, Cotton WR (2012) Potential indirect effects of aerosol on tropical cyclone intensity: Convective fluxes and cold-pool activity. *Atmos Chem Phys Discuss* 12(1):351–385. <https://doi.org/10.5194/acpd-12-351-2012>
- Kurihara Y, Bender MA, Tuleya RE, Ross RJ (1990) Prediction experiments of Hurricane Gloria (1985) using a multiply nested movable mesh model. *Mon Wea Rev* 118(10): 2185–2198. [https://doi.org/10.1175/1520-0493\(1990\)118<2185:peohgu>2.0.co;2](https://doi.org/10.1175/1520-0493(1990)118<2185:peohgu>2.0.co;2)
- Kurihara Y, Bender MA, Ross R (1993) An initialization scheme of hurricane models by vortex specification. *Mon Wea Rev* 121(7): 2030–2045. [https://doi.org/10.1175/1520-0493\(1993\)121<2030:aisohm>2.0.co;2](https://doi.org/10.1175/1520-0493(1993)121<2030:aisohm>2.0.co;2)
- Le Marshall J (1998) Cloud and water vapour motion vectors in tropical cyclone track forecasting—a review. *Meteorol Atmos Phys* 65(3–4):141–151. <https://doi.org/10.1007/BF01030784>
- Marshall JFL, Smith WM, Callan GM (1985) Hurricane Debby—an illustration of the complementary nature of VAS soundings and cloud and water vapor motion winds. *Bull Am Meteorol Soc* 66(3): 258–263. [https://doi.org/10.1175/1520-0477\(1985\)066<0258:HDIOTC>2.0.CO;2](https://doi.org/10.1175/1520-0477(1985)066<0258:HDIOTC>2.0.CO;2)
- Miglietta MM, Moscatello A, Conte D, Mannarini G, Lacorata G, Rotunno R (2011) Numerical analysis of a Mediterranean ‘hurricane’ over south-eastern Italy: sensitivity experiments to sea surface temperature. *Atmos Res* 101(1–2):412–426. <https://doi.org/10.1016/j.atmosres.2011.04.006>
- Panda J, Singh H, Wang PK, Giri RK, Routray A (2015) A qualitative study of some meteorological features during tropical cyclone PHET using satellite observations and WRF modeling system. *J Indian Soc Remote Sens* 43(1):45–56. <https://doi.org/10.1007/s12524-014-0386-4>
- Peng S, Li Y, Gu X, Chen S, Wang D, Wang H, Zhang S, Lv W, Wang C, Liu B, Liu D (2015) A real-time regional forecasting system established for the South China Sea and its performance in the track forecasts of tropical cyclones during 2011–13. *Weather Forecast* 30(2):471–485. <https://doi.org/10.1175/WAF-D-14-00070.1>
- Rai D, Pattnaik S (2018) Sensitivity of tropical cyclone intensity and structure to planetary boundary layer parameterization. *Asia-Pacific J Atmos Sci* 54(3):473–488. <https://doi.org/10.1007/s13143-018-0053-8>
- Roy C, Kovárdányi R (2012) Tropical cyclone track forecasting techniques—A review. *Atmos Res* 104:40–69. <https://doi.org/10.1016/j.atmosres.2011.09.012>

- Skamarock WC, Klemp JB, Dudhia J, Gill DO, Barker DM, Duda MG, Huang XY, Wang W, Powers JG (2008) G.: A description of the Advanced Research WRF version 3. NCAR Tech:Note NCAR/TN-475 + STR
- Tsuboi A, Takemi T, Yoneyama K (2016) Seasonal environmental characteristics for the tropical cyclone genesis in the Indian Ocean during the CINDY2011/DYNAMO field experiment. *Atmos* 7(5):66. <https://doi.org/10.3390/atmos7050066>
- Wang Y, Kepert JD, Holland GJ (2001) The effect of sea spray evaporation on tropical cyclone boundary layer structure and intensity. *Mon Weather Rev* 129(10):2481–500. [https://doi.org/10.1175/1520-0493\(2001\)129<2481:TEOSSE>2.0.CO;2](https://doi.org/10.1175/1520-0493(2001)129<2481:TEOSSE>2.0.CO;2)
- Wu CC, Huang TS, Chou KH (2004) Potential vorticity diagnosis of the key factors affecting the motion of Typhoon Sinlaku (2002). *Mon Weather Rev* 132(8):2084–93. [https://doi.org/10.1175/1520-0493\(2004\)132<2084:PVDOTK>2.0.CO;2](https://doi.org/10.1175/1520-0493(2004)132<2084:PVDOTK>2.0.CO;2)
- Wu L, Chen X (2016) Revisiting the steering principle of tropical cyclone motion in a numerical experiment. *Atmos Chem Phys* 16:14925–14936. <https://doi.org/10.5194/acp-16-14925-2016>
- Wu Y, Chen S, Li W, Fang R, Liu H (2020) Relative vorticity is the major environmental factor controlling tropical cyclone intensification over the Western North Pacific. *Atmos Res* 237:104874. <https://doi.org/10.1016/j.atmosres.2020.104874>
- Xu X, Peng S, Yang X, Xu H, Tong DQ, Wang D, Guo Y, Chan JC, Chen L, Yu W, Li Y (2013) Does warmer China land attract more super typhoons? *Sci Rep* 3(1):1–8. <https://doi.org/10.1038/srep01522>
- Yamada H, Nasuno T, Yanase W, Satoh M (2016) Role of the vertical structure of a simulated tropical cyclone in its motion: a case study of typhoon Fengshen (2008). *SOLA* 12:203–208. <https://doi.org/10.2151/sola.2016-041>
- Yan Z, Ge X, Guo B (2017) Simulated sensitivity of tropical cyclone track to the moisture in an idealized monsoon gyre. *Dyn Atmos Oceans* 80:173–182. <https://doi.org/10.1016/j.dynatmoce.2017.10.008>
- Yue J, Meng Z, Yu CK, Cheng LW (2017) Impact of coastal radar observability on the forecast of the track and rainfall of Typhoon Morakot (2009) using WRF-based ensemble Kalman filter data assimilation. *Adv Atmos Sci* 34:66–78. <https://doi.org/10.1007/s00376-016-6028-8>

Publisher's Note Springer Nature remains neutral with regard to jurisdictional claims in published maps and institutional affiliations.

Authors and Affiliations

Jixin Chen^{1,2} · Chuying Mai¹ · Mingsen Zhou^{1,3} · Shumin Chen^{1,2}  · Weibiao Li^{1,2} ·
Rong Fang¹ · Zhongkuo Zhao³

Jixin Chen
chenjx223@mail2.sysu.edu.cn

Chuying Mai
maichy5@mail2.sysu.edu.cn

Mingsen Zhou
zhoums@gd121.cn

Weibiao Li
eeslwb@mail.sysu.edu.cn

Rong Fang
fangr5@mail2.sysu.edu.cn

Zhongkuo Zhao
zhaozk@gd121.cn

¹ School of Atmospheric Sciences, Sun Yat-sen University, Guangzhou 510275, China

² Southern Laboratory of Ocean Science and Engineering, Zhuhai 519082, China

³ Guangzhou Institute of Tropical and Marine Meteorology, China Meteorological Administration, Guangzhou 510062, China